NeuroImage 124 (2016) 869–875

Contents lists available at ScienceDirect

NeuroImage

journal homepage: www.elsevier.com/locate/ynimg

Reaching with the sixth sense: Vestibular contributions to voluntary motor control in the human right parietal cortex

Alexandra Reichenbach [a,*], Jean-Pierre Bresciani [a,b,c], Heinrich H. Bülthoff [a,d,*], Axel Thielscher [a,e,f]

[a] Max Planck Institute for Biological Cybernetics, Spemannstr. 38, 72076 Tübingen, Germany
[b] Laboratoire de Psychologie et NeuroCognition, University of Grenoble, BP47, 38040 Grenoble, Cedex 9, France
[c] Department of Medicine, University of Fribourg, Boulevard de Pérolles 90, 1700 Fribourg, Switzerland
[d] Dept. of Brain and Cognitive Engineering, Korea University, Anam-dong 5ga, Seonbuk-gu, Seoul 136-713, Republic of Korea
[e] Danish Research Center for Magnetic Resonance, Copenhagen University Hospital, Kettegård Alle 30, 2650 Hvidovre, Denmark
[f] Biomedical Engineering Section, Technical University of Denmark, Anker Engelunds Vej 1, Building 101A, 2800 Kgs. Lyngby, Denmark

ARTICLE INFO

Article history:
Received 13 May 2015
Accepted 20 September 2015
Available online 28 September 2015

Keywords:
Voluntary movement
Sensorimotor integration
Vestibular afferent
Reaching movement
Transcranial magnetic stimulation
Human posterior parietal cortex

ABSTRACT

The vestibular system constitutes the silent sixth sense: It automatically triggers a variety of vital reflexes to maintain postural and visual stability. Beyond their role in reflexive behavior, vestibular afferents contribute to several perceptual and cognitive functions and also support voluntary control of movements by complementing the other senses to accomplish the movement goal. Investigations into the neural correlates of vestibular contribution to voluntary action in humans are challenging and have progressed far less than research on corresponding visual and proprioceptive involvement. Here, we demonstrate for the first time with event-related TMS that the posterior part of the right medial intraparietal sulcus processes vestibular signals during a goal-directed reaching task with the dominant right hand. This finding suggests a qualitative difference between the processing of vestibular vs. visual and proprioceptive signals for controlling voluntary movements, which are pre-dominantly processed in the left posterior parietal cortex. Furthermore, this study reveals a neural pathway for vestibular input that might be distinct from the processing for reflexive or cognitive functions, and opens a window into their investigation in humans.

Introduction

During goal-directed movements, sensory information is continuously integrated into the motor plan in order to ensure and improve execution success (Desmurget and Grafton, 2000; Shadmehr et al., 2010; Wolpert et al., 1995). It is well established that the posterior parietal cortex (PPC) plays a prominent role in processing visual and proprioceptive information for motor control (Culham and Valyear, 2006; Filimon et al., 2009; Heed et al., 2011; Reichenbach et al., 2011; Reichenbach et al., 2014; Shadmehr and Krakauer, 2008), but comparable studies for the vestibular system are still missing.

Humans utilize afferent vestibular information for voluntary movement control, which has been illustrated in a wide range of behavioral studies using passive rotation during reaching (Bresciani et al., 2002b; Bresciani et al., 2005), arm-reaches involving trunk movements (Tunik et al., 2003), and galvanic vestibular stimulation (GVS) during a variety of voluntary movement tasks (Bresciani et al., 2002a; Day, 1999; Day and Reynolds, 2005; Mars et al., 2003). Neuroimaging studies applying GVS (Stephan et al., 2005) or caloric vestibular stimulation (Dieterich et al., 2003; Fasold et al., 2002; Suzuki et al., 2001) indicate that several temporal and parietal areas are involved in processing vestibular input in humans (Lopez and Blanke, 2011). Furthermore, TMS studies have demonstrated that the PPC (Seemungal et al., 2008) and the temporo-parietal junction (Lenggenhager et al., 2006) are critically involved in perceptual tasks relying heavily on vestibular information.

The current study set out to test the involvement of the human PPC in the processing of vestibular information for goal-directed reaching movements. Given the important role of the PPC in sensorimotor control and involvement of parietal regions in vestibular processing, the PPC is a prime candidate for playing a critical role in vestibulo-motor control. We used a reaching task to a memorized visual target in the dark, during which participants bodies were occasionally rotated to the left or to the right. In the absence of visual input, vestibular information needed to be processed to compensate for the passive rotation and achieve the reaching goal. We probed the involvement of different parietal areas in the processing of vestibular information for motor control with interspersed TMS trials. Administering TMS briefly after onset of a sensory perturbation such as the full-body rotation allows for specifically interfering with the fast online control processes integrating recent sensory information (Desmurget et al., 1999; Reichenbach et al., 2011;

* Corresponding authors at: Max Planck Institute for Biological Cybernetics, Spemannstr. 38, 72076 Tübingen, Germany.
E-mail addresses: alex.reichenbach@gmx.de (A. Reichenbach), heinrich.buelthoff@tuebingen.mpg.de (H.H. Bülthoff).

http://dx.doi.org/10.1016/j.neuroimage.2015.09.043

Reichenbach et al., 2014; Tunik et al., 2005). Behavioral deficits after administering TMS demonstrate a causal contribution of the stimulated cortical area to the correction process. In order to enhance the spatial resolution of TMS, we tested a grid of TMS stimulation sites (Busan et al., 2009; Reichenbach et al., 2011; Reichenbach et al., 2014; Striemer et al., 2011) on both hemispheres, which also tightly controls for unspecific TMS side effects.

Material and methods

General procedure

Ten healthy, right-handed volunteers (aged 22–33 years, four females) including one of the authors participated in the study. Besides the author, all participants were naïve about the purpose of the study. They had normal or corrected-to-normal vision and no history of neurological disorders. Written informed consent was obtained from each participant prior to the first experiment. The study was conducted in accordance with the Declaration of Helsinki, and approved by the local ethics committee of the Medical Faculty of the University of Tübingen. Each participant attended two experimental TMS sessions, which were separated one week or more. During the experiments, participants wore earplugs to prevent hearing damage from the TMS clicks and auditory influence on task performance.

A T1-weighted structural image (MPRAGE, TR 1900 ms, TE 2.26 ms, TI 900 ms, flip angle 9°, 192 coronal slices, 1 mm iso-voxel resolution, 2 averages) acquired on a Siemens 3 T TIM Trio (Siemens, Erlangen, Germany) was available for each participant from previous studies.

The experimental sessions were carried out in a completely darkened room, in which the experimentally provided visual information constituted the only guidance for spatial orientation. The visual cues were a body-fixed fixation LED, and a briefly flashing target projection from an earth-fixed laser pointer, to which participants had to perform memory-guided reaching movements with their right hand (Fig. 1, see Supplementary Information S1.1. for additional technical details of the setup). Shortly after hand movement onset, participants were passively rotated 30° to the left or right in one third of the trials, respectively. To preserve reaching accuracy, participants were therefore required to modulate online the arm trajectory to compensate for the ongoing body rotation. We tested whether participants' ability to correct for the rotation was reduced when event-related TMS was applied to distinct brain regions in the posterior parietal cortex (PPC), which were reported in previous studies to be involved in vestibular processing or online movement control (Fig. 2).

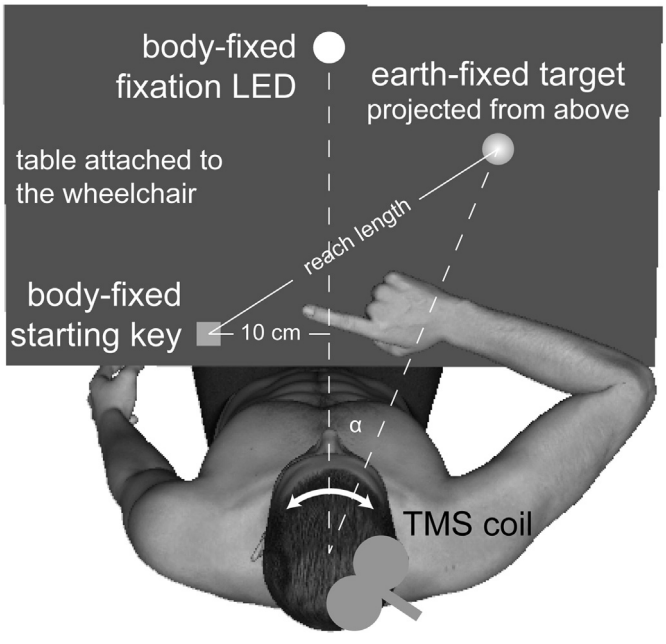

Fig. 1. Schematic experimental setup. The black table was attached to the rotating wheelchair above participant's laps. The starting key and fixation LED were mounted on the table. The target was projected on the table from above via a red laser pointer. As the target position was adjusted to the participant's arm length, the reach length ranged between 14.7 and 28.7 cm. Thus, the eccentricity of the target relative to fixation (α) ranged between 1° and 32°. The TMS coil was mounted on an aluminum frame on the chair, and participants' bodies and heads were fixated within this frame using chin-, forehead rest, and padding pillows.

Behavioral task

The experiment started with two training blocks of 48 trials each to familiarize participants with the task and the TMS stimulation. In each of the two experimental sessions, we tested 10 blocks of 48 trials with the hemisphere of stimulation blocked in a session, and the order of hemispheres counterbalanced across participants. Each of the five TMS stimulation sites was tested twice in a session in a randomized order. A block consisted of 8 repetitions of the full permutation of the factors TMS stimulation (yes/no) and rotation (30° to the left/right/none). The trials within a block were fully randomized to prevent that rotation direction or stimulation was predicted.

A trial started self-paced with depressing the key at the starting position, which switched on the target and the fixation LED. Participants were instructed to keep their eyes on the fixation LED throughout the whole trial in order to suppress eye movements and accompanying indirect vestibular information processing resulting from the vestibulo-ocular reflex (Cullen et al., 1991). Switching off the target after 1 s constituted the "go" cue to initiate the reaching movement. In the rotation trials, the wheelchair started rotating with a raised cosine profile 32 ± 4 ms after the participant released the starting key. A rotation of 30° lasted about 900 ms, culminating to maximal velocities of 50°/s and maximal accelerations of 180°/s^2. In the TMS trials, 4 TMS pulses with an inter-stimulus interval of 20 ms were administered, starting 30 ms after the participant released the starting key. Thus, the TMS stimulation covered the initial acceleration phase of the rotation (see Supplementary Information S1.2. for illustration). A trial was finished 1.5 s after the wheelchair stopped rotating. The fixation LED was then switched off and the wheelchair was rotated back to its starting position. The next trial could then be started after 900 ms earliest. This procedure determined the inter-trial interval (ITI) at a minimum of 5.5 s. Because the

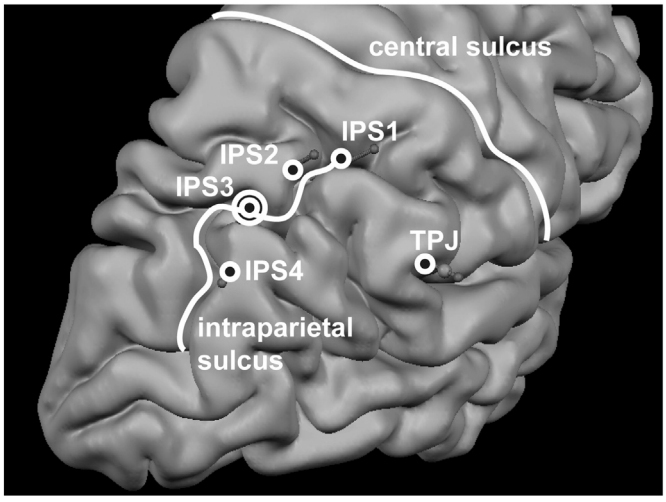

Fig. 2. TMS stimulation sites, rendered on the reconstructed right hemisphere of an exemplarily participant. Adjacent stimulation sites were 1.5–2 cm apart. The stimulation sites on the left hemisphere are exactly mirrored in terms of MNI coordinates. See Supplementary Information S1.3 for MNI coordinates and anatomical correspondence.

start of a trial was self-paced, the real ITI was on average twice as long, resulting in experimental blocks of about 10 min each.

Transcranial magnetic stimulation

A grid of five TMS coil positions on the left parietal cortex and mirror-symmetric five sites on the right parietal cortex (Fig. 2, see Supplementary Information S1.3. for details) were derived from previous fMRI and TMS studies investigating vestibular processing (Dieterich et al., 2003; Seemungal et al., 2008; Stephan et al., 2005), or TMS studies investigating online control during reaching (Chib et al., 2009; Della-Maggiore et al., 2004; Reichenbach et al., 2011; Reichenbach et al., 2014). With these sites, we covered a broad area around the intraparietal sulcus (IPS) and the temporo-parietal junction (TPJ), where processing related to our questions has been localized previously. The distance between adjacent stimulation sites around the IPS ranged between 1.5 and 2 cm, dependent on the participant's head size. This allowed dissociation between different sub-regions of the PPC and the stimulation sites served as mutual control sites.

Biphasic TMS stimuli were applied using a Medtronic MagPro X100 stimulator (MagVenture, Farum, Denmark) with a MC-B70 butterfly coil. The coil position was constantly monitored using a neuronavigation system (BrainView, Fraunhofer IPA, Germany; cf. (Kammer et al., 2007)). The spatial accuracy of the registration between participants' real head and their anatomical MR image in the neuronavigation system was established at the beginning, and checked again at the end of each session using positions of clearly visible landmarks (e.g., nasion and inion). Before each block, the coil was attached to the participants head and carefully tightened to obtain a coil position in the range of 2 mm to the pre-planned stimulation sites. The coil position was constantly monitored within a block and re-adjusted whenever the distance of the coil to the planned stimulation site exceeded 5 mm. The stimulation intensity was chosen to meet two competing goals: It should be as high as possible to maximize the impact on the stimulation site without eliciting direct effects on the primary motor cortex. For this purpose, the coil was placed at the most anterior stimulation site at the beginning of each session, and the intensity was gradually decreased until no more motor responses were elicited in the finger muscles for at least 10 consecutive trials (tested by recording surface EMG from the relaxed first dorsal interosseus). 80% of this intensity was then used as the individual stimulation intensity throughout the session (Reichenbach et al., 2011; Reichenbach et al., 2014). This procedure resulted in stimulation intensities of 32–49% of maximum stimulator output. The coil was initially oriented parallel to the central sulcus and adjusted when necessary.

Data analysis

The beginning of a trial was defined as the time point when the starter key was released, and the end of a trial was defined as the time point when the hand velocity dropped below 2 cm/s. The position data was recorded in earth-fixed coordinates. During post-processing, the positions of every trial were aligned, rotated, and scaled to a unity coordinate system such that the actual starting and target positions were located at 0/0 and 0/100, respectively. The data was then spatially normalized to obtain 100 equidistant data points per reaching trajectory, and averaged over all trials for each condition and participant.

To assess the effect of TMS on the reaching behavior, we compared for each rotation condition the x-component of the trajectories (i.e. the direction perpendicular to the "ideal" straight reaching trajectory) with TMS stimulation to those without TMS stimulation across participants. More specifically, we conducted two-tailed paired t-tests on a significance level of $\alpha = .05$ for each data point. In order to correct for multiple comparisons on dependent data (100 data points per trajectory), we performed a "clusterwise" correction along the reaching trajectory with a permutation test (cf. correction methods for imaging data e.g. Friston et al.(1993)). This means that we assessed how many successive significant t-tests (i.e. the "cluster size" or the length of the trajectory segment) were needed to accept that the trajectories of two conditions are significantly different. To do so, we permuted the data 1000 times over the TMS conditions and stimulation sites independently for each participant (i.e. we re-arranged the labels "TMS condition" and "stimulation site" while leaving the spatial information within trajectories intact), and performed the t-tests for each set of permutations. This procedure yielded the minimum number of successive data points with significant t-tests needed to obtain an overall false positive rate of $\alpha = .05$. In other words, we approximated the distribution of cluster sizes on randomized data in order to find the cluster size threshold that (wrongly) returned a significant difference between trajectories in 5% of the test cases on random data. The same analysis was additionally performed with baseline corrected data, i.e. the corresponding data without wheelchair rotation (with or without TMS stimulation, respectively) was subtracted from the left- and rightward rotations before comparing the trajectories. This procedure removed putative correction-independent TMS effects on the reaching movements. Because we normalized the trajectories to 100 data points, the length of the trajectory segment corresponds to the percentage of the two trajectories being continuously significantly different.

Additionally, we assessed the angular deviation at the end of the reach (*EndAng*), the end accuracy in the direction of the rotation (*EndDevX*) and in the direction of the reach (*EndDevY*), and their respective variability (*EndVarX*, *EndVarY*). Note that the measure *EndAng* remained unaffected from the normalization procedure. Pre-planned pairwise two-tailed t-tests TMS vs. no TMS with Bonferroni correction for the number of stimulation sites (adjusted significance threshold: $\alpha = .005$) on these measures served as additional indicator for sites with significant TMS effects. In order to assess the spatial specificity of significant effects, we subsequently tested whether the TMS effects over affected sites were significantly larger than the average TMS effect across the remaining sites (Oliver et al., 2009; Reichenbach et al., 2014). Compared to a standard omnibus ANOVA, this approach has a higher power to detect significant effects that are localized to a single stimulation site when testing a larger number of sites. Reported values are mean ± SE across subjects.

Results and discussion

General reaching behavior averaged across TMS stimulation sites

All participants successfully performed reaching movements to the remembered target and corrected for the rotation. Averaged over all stimulation sites, the angular reaching error at the end of the movement (*EndAng*) was biased slightly to the right for un-rotated reaches ($3.9 \pm 2.7°$; $t_9 = 1.46$; $p = .178$). For rotated reaches, participants overcorrected both for rotations to the left ($16.8 \pm 3.9°$; $t_9 = 4.28$; $p = .002$) and for rotations to the right ($-12.0 \pm 3.7°$; $t_9 = 3.22$; $p = .010$). While vestibular-evoked overestimations are consistently reported for pure perceptual tasks (Israel et al., 1995; Ivanenko et al., 1997; Jurgens et al., 2003), arm movement accuracy tends to be accurate despite vestibular perturbations (Blouin et al., 2010; Bresciani et al., 2002b; Guillaud et al., 2006). However, behavioral studies with the same setup as used in this study report similar overcorrections in arm position to counteract rotations (Schomaker et al., 2011). Since the main interest of this study was the effect of TMS on the corrective movement, a constant bias in the correction would cancel out in comparing TMS vs. no-TMS trials. The overall movement time (unperturbed: 952 ± 44 ms) was slightly prolonged for rotations to the left (1003 ± 37 ms; $t_9 = 1.81$; $p = .104$), and significantly prolonged for rotations to the right (1068 ± 48 ms; $t_9 = 3.57$; $p = .006$). Note that in the latter condition the correction was opposite to the original reaching direction and thus required the recruitment of additional muscles such as the major pectoralis. Importantly, however, when averaging over all

stimulation sites, TMS had neither an effect on these reaching parameters, nor on reaching end accuracy or variability (see Supplementary Information S2.1. for detailed statistics). Thus, TMS in general did not have any unspecific side effect influencing the movements. Additionally, none of the participants reported any subjective TMS effects apart from weak cutaneous nerve stimulations directly beneath the coil.

TMS over the right posterior mIPS reduced the extent of corrective movements

The main question of the study was whether we can find evidence for processes utilizing vestibular signals for movement corrections in the human parietal cortex. Based on the permutation tests, only conditions in which TMS stimulation resulted in changing a segment spanning at least 37% of the trajectory were accepted as exhibiting a significant TMS effect (28% for the baseline corrected data). The only stimulation site showing such robust TMS effects was the right posterior mIPS (right IPS3, Fig. 3A&B; see also Fig. 3C for an exemplary control site and Supplementary Information S2.3 for all stimulation sites). When TMS was administered over the right IPS3, participants corrected significantly less in the early phase of the movement for rotations to the left (47% difference along the trajectories; $p = .035$, corrected; Fig. 3A), and in the late phase for rotations to the right (44%; $p = .039$, corrected). Whether the temporal dissociation of the TMS effect between rotations to the left and right was driven by differential muscle recruitment or perturbation of different neural processes cannot be resolved with the current study. However, the TMS effect for rotations to the right was more robust, as only this effect remained significant after baseline correction (48%; $p = .015$, corrected; Fig. 3B).

Significant TMS effects on end accuracy for rightward rotations confirmed this finding. Stimulating over the right IPS3 diminished the cumulative correction at the end of the movement as evident from both the deviation in direction of the rotation (*EndDevX*; $t_9 = 4.53$; $p = .001$; $-23.2 \pm 6.4/-27.2 \pm 6.6$; TMS/no TMS), and the angular end deviation (*EndAng*; $t_9 = 3.74$; $p = .005$; $-13.3 \pm 3.1°/-16.2 \pm 3.3°$; TMS/no TMS). In addition, the TMS effect on end accuracy was spatially specific to the right IPS3; it was significantly larger than the TMS effect averaged across all remaining stimulation sites (*EndDevX*; $t_9 = 2.50$; $p = .017$). Corresponding analyses without the participating author did not qualitatively change the results (see Supplementary Information S2.4 for comparison). The more unspecific measures *EndDevY* and endpoint variability (*EndVarX*, *EndVarY*), though, were not influenced by TMS over the right IPS3 (see Supplementary Information S2.6 for detailed statistics). Further exploratory analyses for an influence of individual target eccentricity or hand movement velocity on the TMS efficacy did not reveal a relevant interaction (see Supplementary Information S2.5 for details). Additionally, we found no other stimulation sites with significant TMS effects on the end accuracy measures (*EndDevX*, *EndAng*, *EndDevY*) or their variability (*EndVarX*, *EndVarY*) (see Supplementary Information S2.6 for detailed statistics and S2.7 for further detailed analyses of the within-subject variability). Taken together, the TMS effects represent a robust behavioral impairment stemming from an interference of neural processing specifically on the right posterior mIPS. The human mIPS, probably bilateral, has been suggested to be the functional equivalent to the macaque monkey's parietal reach region (PRR; Grefkes and Fink, 2005; Grefkes et al., 2004). The PRR is considered to be the sensorimotor interface for arm reaching movements (Cohen and Andersen, 2002) and the current findings fit in this framework.

Sensory processing for online motor control

In light of the TMS literature about sensorimotor integration, it seems surprising that the right PPC is the critical structure for processing vestibular input during right-handed reaching. Visual and proprioceptive information about the target and the hand for online control of movements is pre-dominantly processed in the left PPC (Desmurget et al., 1999; Reichenbach et al., 2011; Reichenbach et al., 2014; Tunik et al., 2005), or in the hemisphere contralateral to the acting hand/arm (Rice et al., 2007). Those two sensory modalities, however, provide absolute information about the target and hand positions in eye- or body-centered reference frames (Buneo and Andersen, 2006). Vestibular input provides only relative information about head/body position by supplying movement signals (Cullen, 2012). Hence, vestibular afferences contribute to updating internal representations of the body with respect to the environment, which need to be initiated or calibrated based on other sensory information (Angelaki and Cullen, 2008).

Interestingly, we found the next largest TMS effect on the right anterior mIPS (right IPS2) for un-rotated reaching movements (19%; $p = .083$, corrected; cf. Supplementary Information S2.3. Fig. S4 right panel). This effect is not very pronounced in the present study; however, it closely resembles a previous finding for memory-guided reaching, where TMS over the right PPC resulted in a leftward shift of the reaching endpoint (Vesia et al., 2006). The un-rotated reaches in the present study are similar memory-guided reaching movements, thus this finding constitutes a direct replication of the previous results despite some differences in the experimental protocol between studies. Together, these findings hint towards a functional dissociation between the right anterior and posterior mIPS. The anterior part seems to be crucially involved in maintaining the internal (stationary) target representation

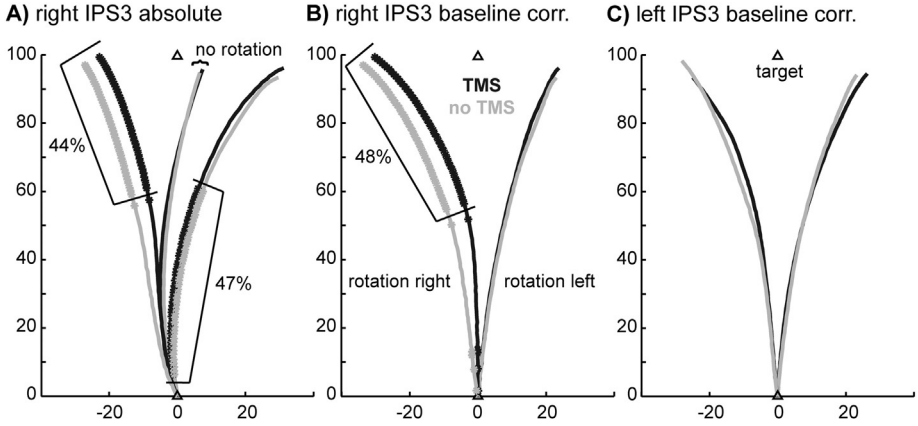

Fig. 3. Average group trajectories illustrating the TMS effects. The axes are arbitrary units, spatially normalized to the individual target positions at 0/100. The stars/bold parts indicate the positions where the x directions differed significantly between TMS (black) and no TMS (grey) trials across participants ($p < .05$, uncorrected). A) Absolute trajectories for TMS stimulation over the right posterior mIPS (right IPS3). See Supplementary Information S2.2 for exemplary non-normalized single subject data. B) Baseline corrected trajectories for TMS stimulation over the right posterior mIPS (right IPS3). C) Exemplary graph illustrating the absence of a TMS effect for the left posterior mIPS (left IPS3), exactly mirrored to the stimulation site of panels a and b. See Supplementary Information S2.3 for graphs of all stimulation sites.

while the posterior part is more specifically concerned with online updating the target representation via indirect signals such as vestibular input or efference signals. This idea is in line with a previous study demonstrating the importance of more posterior parts of the right PPC for updating memorized saccade targets across eye movements (Morris et al., 2007). Importantly, this processing seems to be confined to updating a memorized or internal representation of the target position, since TMS studies investigating the adjustment of reaching movements to a change in the visually perceived target position demonstrate that these corrections are attenuated by TMS over the left PPC (Desmurget et al., 1999; Reichenbach et al., 2011). More specifically, if the same process was updating the target representation based on direct visual information and indirect vestibular signals, we would expect to see a TMS effect for the left anterior IPS (left IPS1), which exactly corresponds to the stimulation site that yielded impairments in the corrective movement for a visual target displacement in the study of Reichenbach et al. (2011).

The alternative explanation that TMS impaired proprioceptive updating of the arm position, which was altered due to Coriolis forces resulting from the rotation (Lackner and DiZio, 2005), is unlikely. If this was the case, we would expect to see TMS effects for the left posterior mIPS (left IPS3), the corresponding stimulation site contralateral to the reaching arm. This left-hemispheric region has been identified as a key region for proprioceptive processing during motor control (Chib et al., 2009; Della-Maggiore et al., 2004; Reichenbach et al., 2014), and the left IPS3 in the present study exactly corresponds to the stimulation site that yielded impairments in the corrective movement for a force-field perturbation in the study of Reichenbach et al. (2014).

Neural substrates of processing vestibular input in the human brain

Neuroimaging studies probing the vestibular system with GVS or CVS report right-hemispheric dominance (Suzuki et al., 2001), dominance of the ipsi-rotational, and the non-dominant hemisphere (Dieterich et al., 2003; Dieterich et al., 2005). Our findings for a TMS effect over the right PPC are in line with these observations: our participants were right-handed (i.e. their right hemisphere is the non-dominant one) and our TMS effects were more robust for rotations to the right (i.e. rotations to the ipsi-lesional side). Therefore, the combination of all these factors likely contributed to the robust behavioral impairments we observed when stimulating the right posterior mIPS while participants experienced rightward rotations. The previous neuroimaging studies, however, illustrate general vestibular processing detached from behavior while the present study demonstrates the functional importance of the right posterior mIPS for vestibular processing during a motor task.

A behavioral dissociation of vestibular processing for reflexive behavior vs. cognitive tasks has been recently suggested by demonstrating differential processing of vestibular signals as early as in the cerebellum (see Seemungal (2014) for a review). Processing vestibular input for voluntary motor control is still missing in this picture. Interestingly, Seemungal et al. (2008) observe just the opposite effect to our findings in a cognitive task: They disrupted path-integration during a vestibular navigation task for rotations contra-lateral to the hemisphere stimulated with TMS. This finding might appear puzzling in light of our results and the literature cited above. However, navigation-like behavior investigated in that study has been suggested to rely on different processing than online control based on vestibular information (Bresciani et al., 2002b). This is in line with neuroanatomical studies suggesting that the functional network subserving sensorimotor integration is rather distinct from the network subserving spatial navigation, with the latter mainly comprising the hippocampus and bilateral parietal regions (Iaria et al., 2007; Maguire et al., 1998; Morris et al., 1982). Taken together, it is possible that the neural pathway processing vestibular input for voluntary motor control might form a third dissociable network for vestibular processing. However, its delineation from and interaction with reflexive and cognitive vestibular networks remains to be investigated.

The human IPS has been implicated for vestibular processing (see Lopez and Blanke (2011) for a recent review) but this region seems to be secondary regarding to meta-analyses on the quest for a "human vestibular cortex" (Lopez et al., 2012; zu Eulenburg et al., 2012). In light of the differential purpose of primary sensory vs. sensorimotor areas and corresponding differentiation in other sensory modalities, one would not necessarily expect that vestibulo-motor areas are located directly within the vestibular core network. Thus, the present study helps to extend our knowledge about the functional contribution of secondary cortical regions involved in vestibular processes beyond the vestibular core network.

Control for unspecific TMS effects

Using individually adjusted stimulation intensities, we carefully ruled out that TMS caused direct motor impairments that would have biased our results. Direct influence of TMS on M1 would be primarily expected for TMS stimulation sites on the left hemisphere, as all our participants were right handed and reached with their right hand. However, TMS was effective in disturbing reaching performance for a coil position above the right hemisphere. In addition, the absence of TMS effects when stimulating adjacent sites with equal or closer proximity to M1 render the possibility of any unspecific TMS effect very unlikely. The analyses of the movement times served as additional control. TMS never prolonged the reaching time for any stimulation site, even for the stimulation site on which we found a spatial effect. To summarize, the observed TMS effects demonstrate a specific disturbance of vestibular processing for the online corrections of the reaching movements, and cannot stem from unspecific TMS effects.

Limitations of the present study

This study constitutes the first investigation into the neural processes that integrate vestibular input into the sensorimotor feedback loop for voluntary motor control in the human brain. As such, it raises many more questions than it can answer. Here, we demonstrate that processes in the right parietal cortex utilize vestibular signals for adjusting voluntary arm movements. It is on future studies to disentangle those neural processes from pathways subserving vestibular processing for reflexes or cognition, and to elucidate potential differential processing for the spatial target location or the acting effector. Moreover, in most natural situations vestibular processing is almost exclusively multisensory (Angelaki and Cullen, 2008) and tightly coupled to efferent signals from body movements (Cullen, 2012). Studies on the interaction between these processes constitute a vast field that awaits exploration.

In our experimental paradigm, participants were instructed to keep gaze on a body-fixed fixation point, which suppresses the vestibular-ocular reflex (Cullen et al., 1991). However, this suppression effect is neither perfect nor complete. Since we did not record eye movements, we cannot exclude that some interaction between eye movements and TMS might have at least partially contributed to the observed TMS effects. Processing of reaching and saccade related information is closely intertwined in the human mIPS (Vesia et al., 2010), therefore it is possible that TMS had a differential effect on potential eye movements in the different conditions.

Furthermore, we have tried to isolate the manipulation of vestibular ex-afferent signals from the semi-circular canals as much as possible from other sensory or motor input. However, due to the necessity to tilt participants' heads in the setup we could not avoid a residual otolith stimulation that was not controlled for. A recent study demonstrated the involvements of the adjacent right supramarginal gyrus in the perception of the subjective visual vertical, a cognitive task for which visual information has to be combined with the otolith signal (Kheradmand et al., 2015)

and we cannot exclude the possibility that propagation of the stimulation to this area might have biased our results.

Finally, participants were not tested for vestibular function but we relied on self-report about the absence of any neurological disorders. Thus, we can neither exclude the possibility that a participant suffered from mild vestibular impairment nor relate the individual results to other measures of vestibular function.

Conclusions

Our results demonstrate for the first time that neural processes in the human right posterior mIPS utilize ex-afferent vestibular signals for adjusting goal-directed voluntary arm movements on the fly. These findings suggest that vestibular input during voluntary motor control is processed more similarly to internal signals such as the efference copy from motor commands than to other sensory input that provides direct information about movement relevant states such as target and hand positions. Since vestibular afferents signal only *changes* in head and body position except for the direction of gravity in case of the otoliths, their main functional contribution to voluntary motor control is the maintenance of a spatial representation of the body in the environment, similarly to efference signals that provide information about one's own movement in space.

Our findings further corroborate that processing of vestibular input for voluntary motor control is subserved by neural mechanisms distinct from the processing pathways for reflexive behavior or vestibular cognition. We suggest that the human brain features at least three partially dissociable neural pathways processing vestibular signals for different functions: reflexive behavior, voluntary motor control, and perceptual/cognitive tasks. This study therefore opens a window for investigating the neural underpinnings of vestibular processes for voluntary motor control in the human brain. There are of course limitations to this approach considering that core parts of the vestibular network are buried in the depth of the brain (Brandt and Dieterich, 1999), but some higher-level vestibulo-motor processes are accessible on the parietal cortex as demonstrated with this study.

Acknowledgments

This research was funded by a PhD scholarship from the Max Planck Society to A.R., and by the WCU (World Class University) and BK21 PLUS Program through the National Research Foundation of Korea funded by the Ministry of Education. We are thankful to Betty Mohler and Joachim Tesch for their assistance with the technical setup, and to Sonja Cornelsen for her help in data acquisition. The experiment was realized using Cogent Graphics developed by John Romaya at the LON at the Wellcome Department of Imaging Neuroscience, University College London, UK.

Appendix A. Supplementary data

Supplementary data to this article can be found online at http://dx.doi.org/10.1016/j.neuroimage.2015.09.043.

References

Angelaki, D.E., Cullen, K.E., 2008. Vestibular system: the many facets of a multimodal sense. Annu. Rev. Neurosci. 31, 125–150.
Blouin, J., Guillaud, E., Bresciani, J.P., Guerraz, M., Simoneau, M., 2010. Insights into the control of arm movement during body motion as revealed by EMG analyses. Brain Res. 1309, 40–52.
Brandt, T., Dieterich, M., 1999. The vestibular cortex. Its locations, functions, and disorders. Ann. N. Y. Acad. Sci. 871, 293–312.
Bresciani, J.P., Blouin, J., Popov, K., Bourdin, C., Sarlegna, F., Vercher, J.L., Gauthier, G.M., 2002a. Galvanic vestibular stimulation in humans produces online arm movement deviations when reaching towards memorized visual targets. Neurosci. Lett. 318, 34–38.
Bresciani, J.P., Blouin, J., Sarlegna, F., Bourdin, C., Vercher, J.L., Gauthier, G.M., 2002b. Online versus off-line vestibular-evoked control of goal-directed arm movements. Neuroreport 13, 1563–1566.
Bresciani, J.P., Gauthier, G.M., Vercher, J.L., Blouin, J., 2005. On the nature of the vestibular control of arm-reaching movements during whole-body rotations. Exp. Brain Res. 164, 431–441.
Buneo, C.A., Andersen, R.A., 2006. The posterior parietal cortex: sensorimotor interface for the planning and online control of visually guided ovements. Neuropsychologia 44, 2594–2606.
Busan, P., Barbera, C., Semenic, M., Monti, F., Pizzolato, G., Pelamatti, G., Battaglini, P.P., 2009. Effect of transcranial magnetic stimulation (TMS) on parietal and premotor cortex during planning of reaching movements. PLoS One 4, e4621.
Chib, V.S., Krutky, M.A., Lynch, K.M., Mussa-Ivaldi, F.A., 2009. The separate neural control of hand movements and contact forces. J. Neurosci. 29, 3939–3947.
Cohen, Y.E., Andersen, R.A., 2002. A common reference frame for movement plans in the posterior parietal cortex. Nat. Rev. Neurosci. 3, 553–562.
Culham, J.C., Valyear, K.F., 2006. Human parietal cortex in action. Curr. Opin. Neurobiol. 16, 205–212.
Cullen, K.E., 2012. The vestibular system: multimodal integration and encoding of self-motion for motor control. Trends Neurosci. 35, 185–196.
Cullen, K.E., Belton, T., McCrea, R.A., 1991. A non-visual mechanism for voluntary cancellation of the vestibulo-ocular reflex. Exp. Brain Res. 83, 237–252.
Day, B.L., 1999. Galvanic vestibular stimulation: new uses for an old tool. J. Physiol. 517 (Pt 3), 631.
Day, B.L., Reynolds, R.F., 2005. Vestibular reafference shapes voluntary movement. Curr. Biol. 15, 1390–1394.
Della-Maggiore, V., Malfait, N., Ostry, D.J., Paus, T., 2004. Stimulation of the posterior parietal cortex interferes with arm trajectory adjustments during the learning of new dynamics. J. Neurosci. 24, 9971–9976.
Desmurget, M., Grafton, S., 2000. Forward modeling allows feedback control for fast reaching movements. Trends Cogn. Sci. 4, 423–431.
Desmurget, M., Epstein, C.M., Turner, R.S., Prablanc, C., Alexander, G.E., Grafton, S.T., 1999. Role of the posterior parietal cortex in updating reaching movements to a visual target. Nat. Neurosci. 2, 563–567.
Dieterich, M., Bense, S., Lutz, S., Drzezga, A., Stephan, T., Bartenstein, P., Brandt, T., 2003. Dominance for vestibular cortical function in the non-dominant hemisphere. Cereb. Cortex 13, 994–1007.
Dieterich, M., Bense, S., Stephan, T., Brandt, T., Schwaiger, M., Bartenstein, P., 2005. Medial vestibular nucleus lesions in Wallenberg's syndrome cause decreased activity of the contralateral vestibular cortex. Ann. N. Y. Acad. Sci. 1039, 368–383.
Fasold, O., von Brevern, M., Kuhberg, M., Ploner, C.J., Villringer, A., Lempert, T., Wenzel, R., 2002. Human vestibular cortex as identified with caloric stimulation in functional magnetic resonance imaging. NeuroImage 17, 1384–1393.
Filimon, F., Nelson, J.D., Huang, R.S., Sereno, M.I., 2009. Multiple parietal reach regions in humans: cortical representations for visual and proprioceptive feedback during on-line reaching. J. Neurosci. 29, 2961–2971.
Friston, K., Worsley, K.J., Frackowiak, R.S., Mazziotta, J., Evans, A., 1993. Assessing the significance of focal activations using their spatial extent. Hum. Brain Mapp. 1, 210–220.
Grefkes, C., Fink, G.R., 2005. The functional organization of the intraparietal sulcus in humans and monkeys. J. Anat. 207, 3–17.
Grefkes, C., Ritzl, A., Zilles, K., Fink, G.R., 2004. Human medial intraparietal cortex subserves visuomotor coordinate transformation. NeuroImage 23, 1494–1506.
Guillaud, E., Simoneau, M., Gauthier, G., Blouin, J., 2006. Controlling reaching movements during self-motion: body-fixed versus Earth-fixed targets. Mot. Control. 10, 330–347.
Heed, T., Beurze, S.M., Toni, I., Roder, B., Medendorp, W.P., 2011. Functional rather than effector-specific organization of human posterior parietal cortex. J. Neurosci. 31, 3066–3076.
Iaria, G., Chen, J.K., Guariglia, C., Ptito, A., Petrides, M., 2007. Retrosplenial and hippocampal brain regions in human navigation: complementary functional contributions to the formation and use of cognitive maps. Eur. J. Neurosci. 25, 890–899.
Israel, I., Sievering, D., Koenig, E., 1995. Self-rotation estimate about the vertical axis. Acta Otolaryngol. 115, 3–8.
Ivanenko, Y., Grasso, R., Israel, I., Berthoz, A., 1997. Spatial orientation in humans: perception of angular whole-body displacements in two-dimensional trajectories. Exp. Brain Res. 117, 419–427.
Jurgens, R., Nasios, G., Becker, W., 2003. Vestibular, optokinetic, and cognitive contribution to the guidance of passive self-rotation toward instructed targets. Exp. Brain Res. 151, 90–107.
Kammer, T., Vorwerg, M., Herrnberger, B., 2007. Anisotropy in the visual cortex investigated by neuronavigated transcranial magnetic stimulation. NeuroImage 36, 313–321.
Kheradmand, A., Lasker, A., Zee, D.S., 2015. Transcranial magnetic stimulation (TMS) of the supramarginal gyrus: a window to perception of upright. Cereb. Cortex 25, 765–771.
Lackner, J.R., DiZio, P., 2005. Motor control and learning in altered dynamic environments. Curr. Opin. Neurobiol. 15, 653–659.
Lenggenhager, B., Smith, S.T., Blanke, O., 2006. Functional and neural mechanisms of embodiment: importance of the vestibular system and the temporal parietal junction. Rev. Neurosci. 17, 643–657.
Lopez, C., Blanke, O., 2011. The thalamocortical vestibular system in animals and humans. Brain Res. Rev. 67, 119–146.
Lopez, C., Blanke, O., Mast, F.W., 2012. The human vestibular cortex revealed by coordinate-based activation likelihood estimation meta-analysis. Neuroscience 212, 159–179.
Maguire, E.A., Burgess, N., Donnett, J.G., Frackowiak, R.S., Frith, C.D., O'Keefe, J., 1998. Knowing where and getting there: a human navigation network. Science 280, 921–924.

Mars, F., Archambault, P.S., Feldman, A.G., 2003. Vestibular contribution to combined arm and trunk motion. Exp. Brain Res. 150, 515–519.
Morris, R.G., Garrud, P., Rawlins, J.N., O'Keefe, J., 1982. Place navigation impaired in rats with hippocampal lesions. Nature 297, 681–683.
Morris, A.P., Chambers, C.D., Mattingley, J.B., 2007. Parietal stimulation destabilizes spatial updating across saccadic eye movements. Proc. Natl. Acad. Sci. U. S. A. 104, 9069–9074.
Oliver, R., Bjoertomt, O., Driver, J., Greenwood, R., Rothwell, J., 2009. Novel 'hunting' method using transcranial magnetic stimulation over parietal cortex disrupts visuospatial sensitivity in relation to motor thresholds. Neuropsychologia 47, 3152–3161.
Reichenbach, A., Bresciani, J.P., Peer, A., Bülthoff, H.H., Thielscher, A., 2011. Contributions of the PPC to online control of visually guided reaching movements assessed with fMRI-guided TMS. Cereb. Cortex 21, 1602–1612.
Reichenbach, A., Thielscher, A., Peer, A., Bülthoff, H.H., Bresciani, J.P., 2014. A key region in the human parietal cortex for processing proprioceptive hand feedback during reaching movements. NeuroImage 84, 615–625.
Rice, N.J., Tunik, E., Cross, E.S., Grafton, S.T., 2007. On-line grasp control is mediated by the contralateral hemisphere. Brain Res. 1175, 76–84.
Schomaker, J., Tesch, J., Bulthoff, H.H., Bresciani, J.P., 2011. It is all me: the effect of viewpoint on visual–vestibular recalibration. Exp. Brain Res. 213, 245–256.
Seemungal, B.M., 2014. The cognitive neurology of the vestibular system. Curr. Opin. Neurol. 27, 125–132.
Seemungal, B.M., Rizzo, V., Gresty, M.A., Rothwell, J.C., Bronstein, A.M., 2008. Posterior parietal rTMS disrupts human Path Integration during a vestibular navigation task. Neurosci. Lett. 437, 88–92.
Shadmehr, R., Krakauer, J.W., 2008. A computational neuroanatomy for motor control. Exp. Brain Res. 185, 359–381.
Shadmehr, R., Smith, M.A., Krakauer, J.W., 2010. Error correction, sensory prediction, and adaptation in motor control. Annu. Rev. Neurosci. 33, 89–108.
Stephan, T., Deutschlander, A., Nolte, A., Schneider, E., Wiesmann, M., Brandt, T., Dieterich, M., 2005. Functional MRI of galvanic vestibular stimulation with alternating currents at different frequencies. NeuroImage 26, 721–732.
Striemer, C.L., Chouinard, P.A., Goodale, M.A., 2011. Programs for action in superior parietal cortex: a triple-pulse TMS investigation. Neuropsychologia 49, 2391–2399.
Suzuki, M., Kitano, H., Ito, R., Kitanishi, T., Yazawa, Y., Ogawa, T., Shiino, A., Kitajima, K., 2001. Cortical and subcortical vestibular response to caloric stimulation detected by functional magnetic resonance imaging. Brain Res. Cogn. Brain Res. 12, 441–449.
Tunik, E., Poizner, H., Levin, M.F., Adamovich, S.V., Messier, J., Lamarre, Y., Feldman, A.G., 2003. Arm–trunk coordination in the absence of proprioception. Exp. Brain Res. 153, 343–355.
Tunik, E., Frey, S.H., Grafton, S.T., 2005. Virtual lesions of the anterior intraparietal area disrupt goal-dependent on-line adjustments of grasp. Nat. Neurosci. 8, 505–511.
Vesia, M., Monteon, J.A., Sergio, L.E., Crawford, J.D., 2006. Hemispheric asymmetry in memory-guided pointing during single-pulse transcranial magnetic stimulation of human parietal cortex. J. Neurophysiol. 96, 3016–3027.
Vesia, M., Prime, S.L., Yan, X., Sergio, L.E., Crawford, J.D., 2010. Specificity of human parietal saccade and reach regions during transcranial magnetic stimulation. J. Neurosci. 30, 13053–13065.
Wolpert, D.M., Ghahramani, Z., Jordan, M.I., 1995. An internal model for sensorimotor integration. Science 269, 1880–1882.
zu Eulenburg, P., Caspers, S., Roski, C., Eickhoff, S.B., 2012. Meta-analytical definition and functional connectivity of the human vestibular cortex. NeuroImage 60, 162–169.

Supplementary Information to

Reaching with the sixth sense: vestibular contributions to voluntary motor control in the human right parietal cortex

Alexandra Reichenbach, Jean-Pierre Bresciani, Heinrich H. Bülthoff, Axel Thielscher

S1. Supplementary Material and Methods

S1.1. Technical Setup

The experiment took place in the 12x12m Cyberneum Tracking Lab (MPI Tübingen; http://www.cyberneum.de/research-facilities/trackinglab.html), in which the position of infrared-reflective rigid-body marker objects can be identified in 3D using an optical tracking system of 16 infrared Vicon MX13 cameras (Vicon Motion Systems, Oxford, UK). Tracking and recording of objects was accomplished using ViconTracker software with a sampling rate of 120Hz. Participants sat comfortably in a robotic wheelchair capable of 360° rotations (BlueBotics, Lausanne, Switzerland; http://www.cyberneum.de/de/technische-ausstattung/treadmills-more.html). The position and orientation of the participants' right hand and the wheelchair was tracked using four Vicon markers each (Schomaker et al., 2011). A black table was mounted above the participants lap (Fig. 1), on which a keypad was fixated in the bottom left corner (hand starting position), and a white LED on the middle top (body-fixed visual fixation). Additionally, an earth-fixed red laser pointer from above indicated the target position on the table in the top right corner. The distance of the target with respect to the starting position was adjusted for each

subject individually to accommodate for different arm lengths. For fixating the participants' body and head with respect to the wheelchair and stably attaching the TMS coil, a custom-built black aluminium frame was mounted on the chair. A chin and forehead rest fixated the head above the rotation axis with the head tilted downward to allow direct line of sight on the fixation LED and the target. The TMS coil was attached on the frame at one side of the head. Control over the experiment and data recording was accomplished using custom-written MATLAB routines (The MathWorks, Natick, MA, USA) incorporating Cogent 2000 (University College London, London, UK).

S1.2. Trial Timing and Rotation Profile

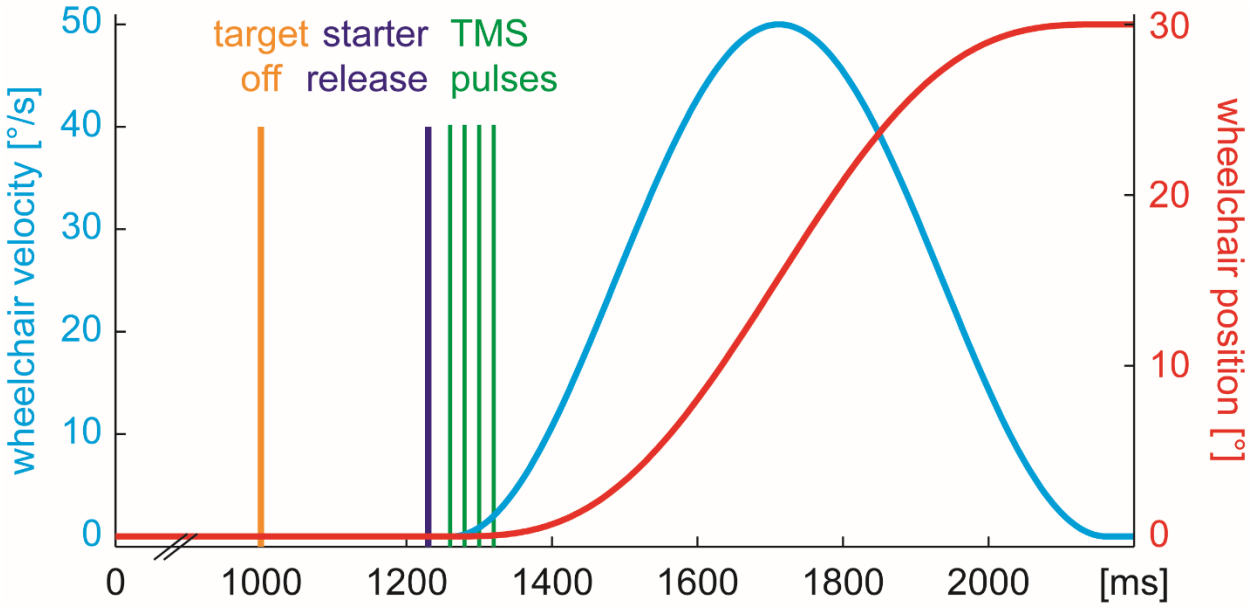

Figure S1 Schematics of the timing of one trial, aligned to the initiation of the trial (start button press, which triggered switching on the fixation and target LEDs). Velocity and position of the wheelchair is exemplary depicted for a +30° rotation.

S1.3. TMS Stimulation Sites

All TMS sites were chosen because processing of vestibular information or sensory processing for online motor control during reaching has been reported on either the site itself or the mirror-symmetric site on the other hemisphere. Furthermore, we tried to cover a large area over the PPC with roughly equidistantly distributed stimulation sites, mirrored across hemispheres.

The MNI coordinates of the grid were transformed from MNI space (Mazziotta et al., 2001) to the space of the individual structural images using the linear registration (FLIRT) of FSL 4.0 (FMRIB, Oxford, UK; (Smith et al., 2005; Smith et al., 2004). The closest coil position on the skull of every participant was determined for each coil position using custom-written MATLAB routines and the surface reconstruction of the skull as obtained with BrainVoyager 2000 (Brain Innovation, Maastricht, The Netherlands).

- Left (right) IPS1 (MNI (x/y/z) [mm]: -(+)44/-42/55), anatomical: anterior IPS
  Reason for inclusion in the study: TMS studies on visual (Reichenbach et al., 2011) and multi-sensory (Reichenbach et al., 2014) processing have identified the left aIPS as a key region for sensory processing during online motor control.
- Left (right) IPS2 (MNI (x/y/z) [mm]: -(+)30/-30/50), anatomical: anterior part of medial IPS[1]
  Reason for inclusion in the study: consistent bilateral fMRI activation during galvanic vestibular stimulation (Stephan et al., 2005). The coordinates are based on the cluster peak in the left hemisphere but the cluster peak in the right hemisphere is located within 5mm distance as well.

[1] The medial IPS (mIPS) has been suggested as the human homologue to the parietal reach region (PRR) Grefkes, C., Fink, G.R., 2005. The functional organization of the intraparietal sulcus in humans and monkeys. J Anat 207, 3-17.

- Left (right) IPS3 (MNI (x/y/z) [mm]: -(+)36/-64/54), anatomical: posterior part of mIPS[1]
  Reason for inclusion in the study: TMS studies have identified the left posterior mIPS as a key region for proprioceptive processing for motor control (Chib et al., 2009; Della-Maggiore et al., 2004; Reichenbach et al., 2014). Additionally, fMRI activation in the left and right posterior mIPS during caloric vestibular stimulation peaked within less than 10mm of the stimulation site (Suzuki et al., 2001).
- Left (right) IPS4 (MNI (x/y/z) [mm]: -(+)40/-76/47), anatomical: caudal IPS, angular gyrus
  Reason for inclusion in the study: TMS over P3/P4[2] disrupted path integration during a vestibular navigation task (Seemungal et al., 2008).
- Left (right) TPJ (MNI (x/y/z) [mm]: -(+)72/-38/36), anatomical: temporo-parietal junction
  Reason for inclusion in the study: consistent (bilateral) fMRI activation during caloric vestibular stimulation (Dieterich et al., 2003). The coordinates are based on the cluster peak in the left hemisphere but the cluster peak in the right hemisphere is located within 9mm distance as well.

[2] P3/P4 corresponds to our stimulation sites IPS4 according to Okamoto, M., Dan, H., Sakamoto, K., Takeo, K., Shimizu, K., Kohno, S., Oda, I., Isobe, S., Suzuki, T., Kohyama, K., Dan, I., 2004. Three-dimensional probabilistic anatomical cranio-cerebral correlation via the international 10-20 system oriented for transcranial functional brain mapping. Neuroimage 21, 99-111.

S2. Supplementary Data

S2.1. Reaching Behavior Averaged Across TMS Stimulation Sites

Mean summary statistics averaged across all stimulation sites (mean (SEM)).

		EndAng [°]	EndDevX	EndDevY	EndVarX	EndVarY	MT [ms]
no rotation	TMS	4.0 (2.6)	6.7 (4.5)	98.6 (3.0)	10.7 (0.8)	9.0 (0.8)	945 (47)
	no TMS	3.7 (2.7)	6.2 (4.6)	97.7 (2.7)	10.4(0.9)	10.3 (1.4)	960 (41)
	TMS effect	$t_9 = 1.53$	$t_9 = 1.38$	$t_9 = 1.84$	$t_9 = 1.01$	$t_9 = 1.24$	$t_9 = 1.12$
		$p = .161$	$p = .202$	$p = .098$	$p = .337$	$p = .247$	$p = .292$
rotation left	TMS	16.8 (3.9)	30.4 (7.2)	96.3 (3.6)	19.5 (1.8)	15.2 (1.7)	993 (38)
	no TMS	16.7 (3.9)	29.7 (7.1)	95.5 (3.3)	19.8 (2.4)	15.2 (1.6)	1013 (38)
	TMS effect	$t_9 = 0.21$	$t_9 = 0.60$	$t_9 = 1.19$	$t_9 = 0.24$	$t_9 = 0.02$	$t_9 = 1.63$
		$p = .837$	$p = .565$	$p = .265$	$p = .816$	$p = .986$	$p = .137$
rotation right	TMS	-11.8 (3.5)	-20.6 (6.8)	99.2 (5.2)	19.9 (3.3)	17.6 (3.1)	1071 (50)
	no TMS	-12.1 (3.9)	-21.0 (7.6)	98.6 (5.8)	18.8 (3.0)	15.6 (1.7)	1065 (47)
	TMS effect	$t_9 = 0.36$	$t_9 = 0.29$	$t_9 = 0.64$	$t_9 = 1.06$	$t_9 = 0.99$	$t_9 = 0.66$
		$p = .731$	$p = .782$	$p = .541$	$p = .318$	$p = .348$	$p = .528$

S2.2. Exemplary Non-normalized Single Subject Trajectories

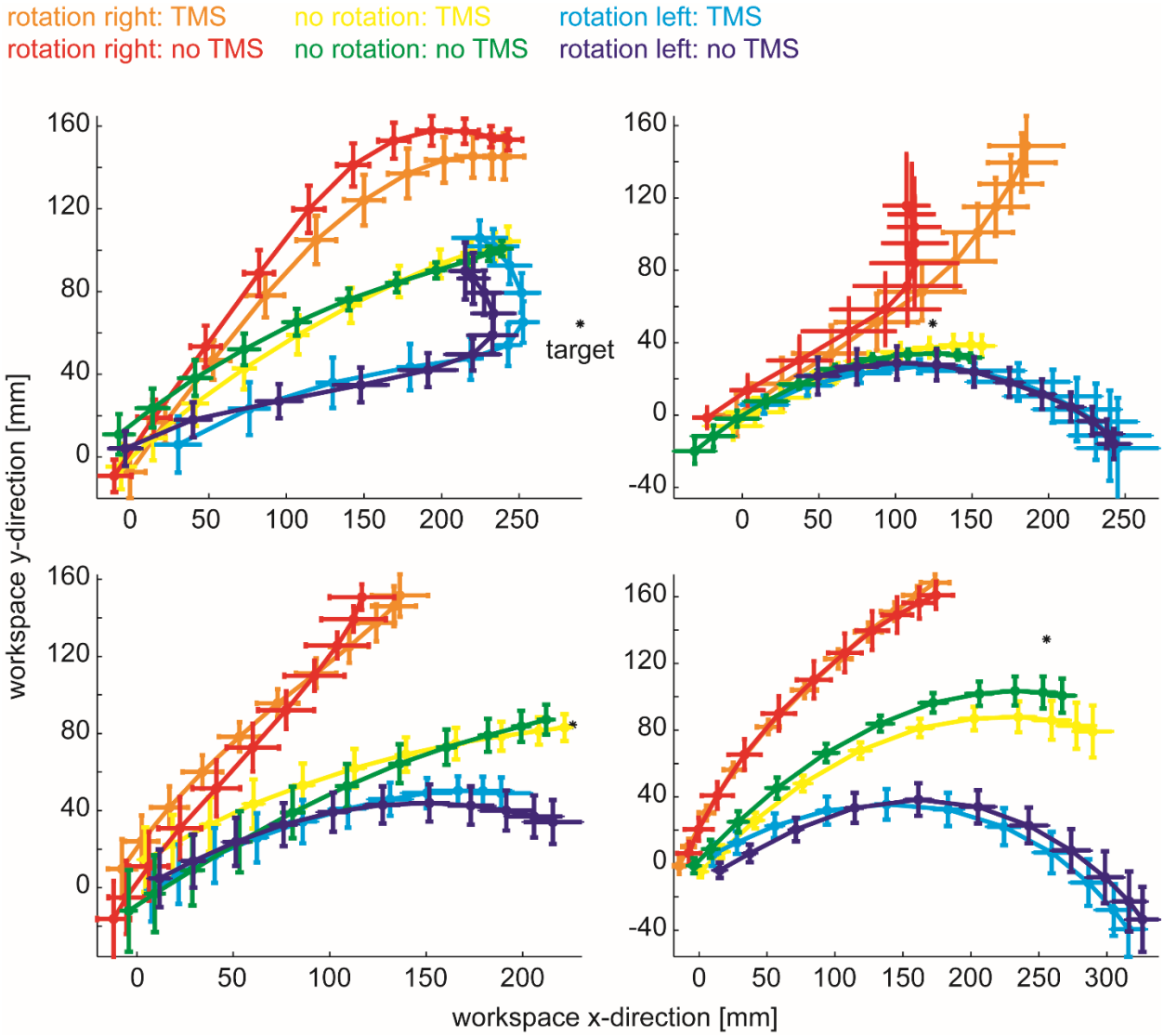

Figure S2 Non-normalized trajectory data for a single experimental block for 4 exemplary participants for TMS stimulation site right IPS3 in world coordinates relative to movement start. The error bars denote ± 1 SEM.

S2.3. Average Group Trajectories for All Stimulation Sites

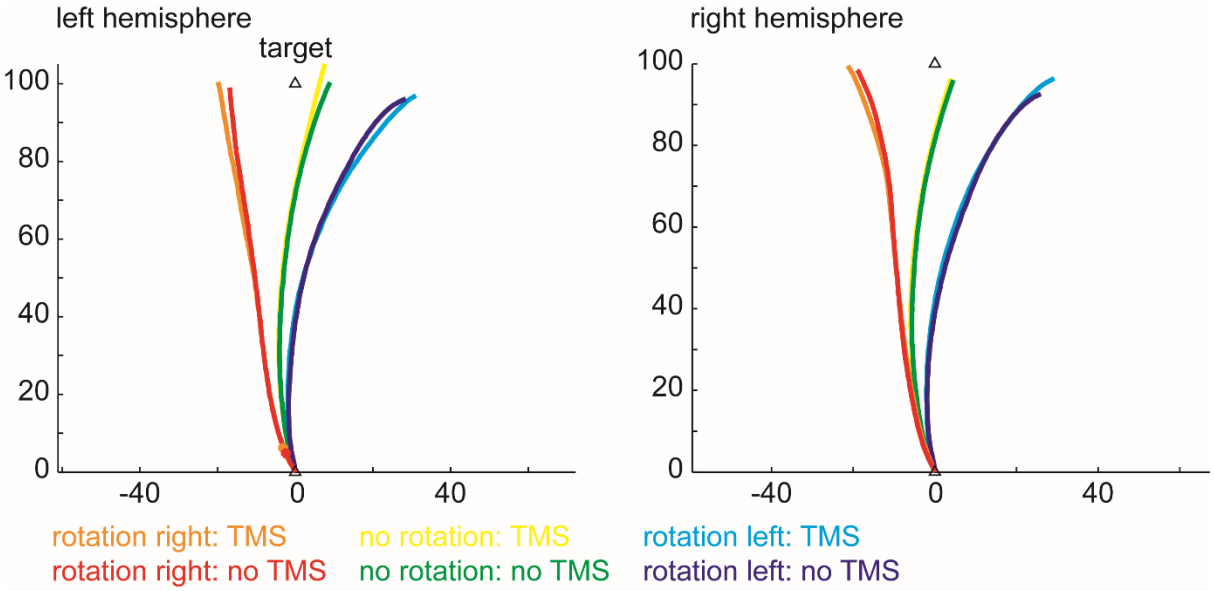

Figure S3 Average group trajectories for the TMS stimulation sites IPS1. The axes are arbitrary units, spatially normalized to the individual target positions at 0/100. The stars / bold parts indicate the positions where the x directions differed significantly between TMS and no TMS trials across participants ($p < .05$, uncorrected).

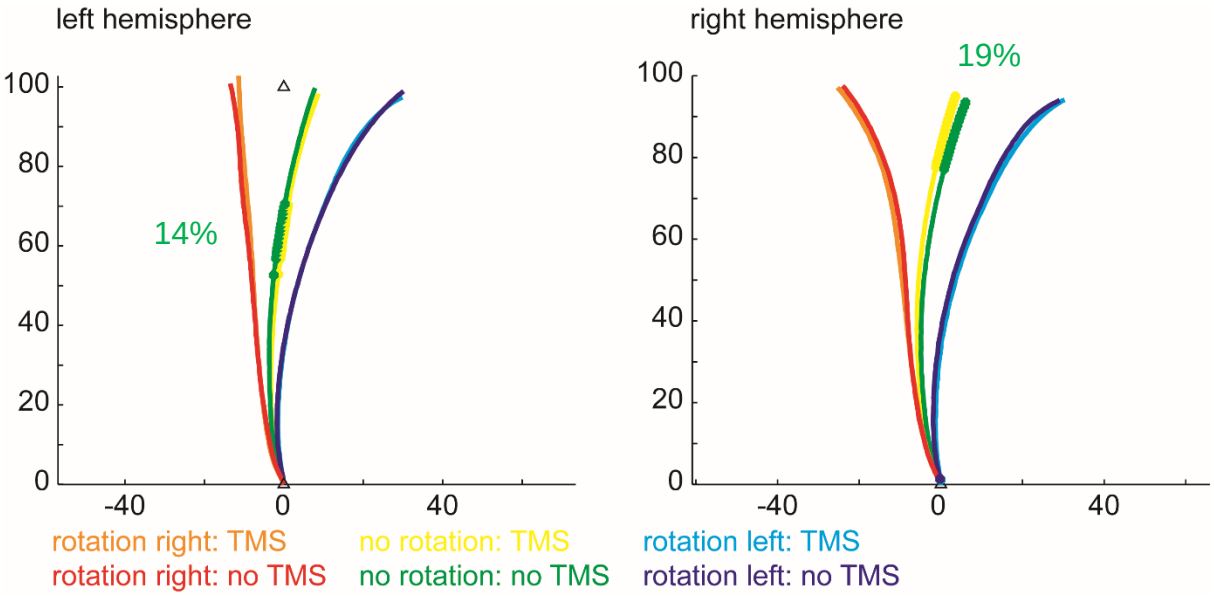

Figure S4 Average group trajectories for the TMS stimulation sites IPS2. Conventions analogue to Fig. S3. Note that the percentage indicates the proportion of **successive** significant tests.

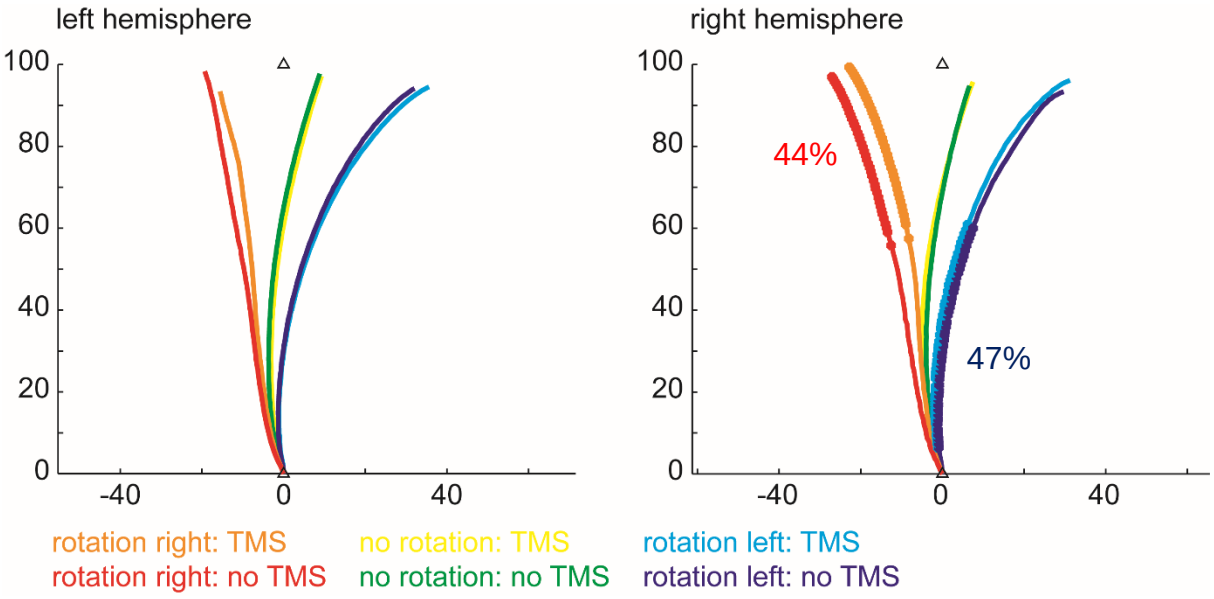

Figure S5 Average group trajectories for the TMS stimulation sites IPS3. Conventions analogue to Fig. S3. Note that the percentage indicates the proportion of **successive** significant tests.

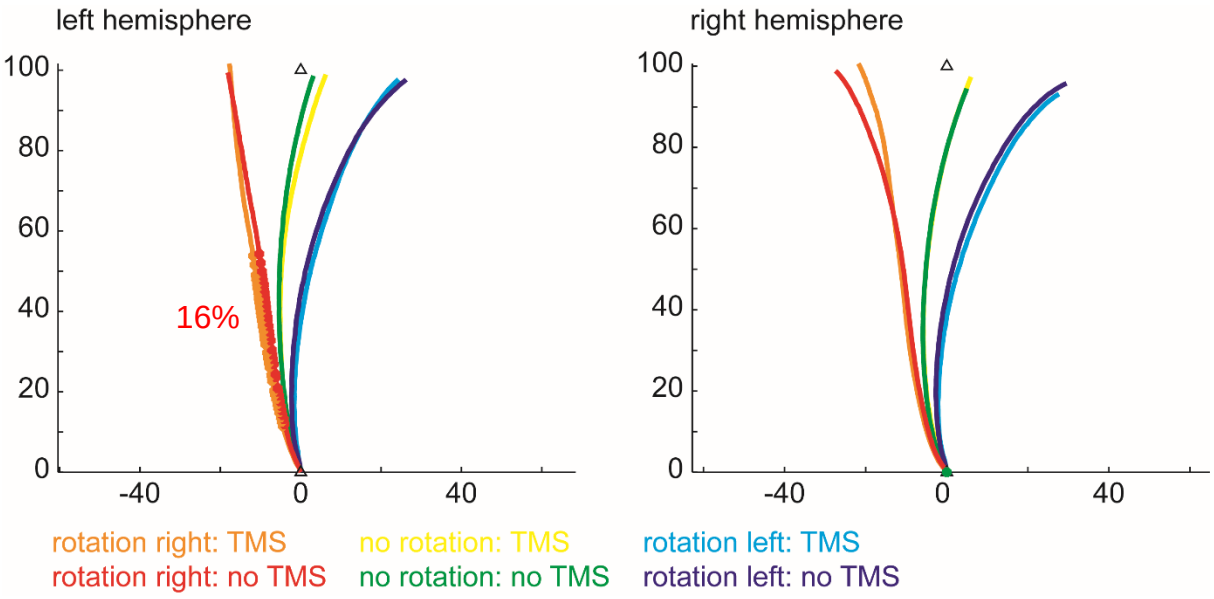

Figure S6 Average group trajectories for the TMS stimulation sites IPS4. Conventions analogue to Fig. S3. Note that the percentage indicates the proportion of **successive** significant tests.

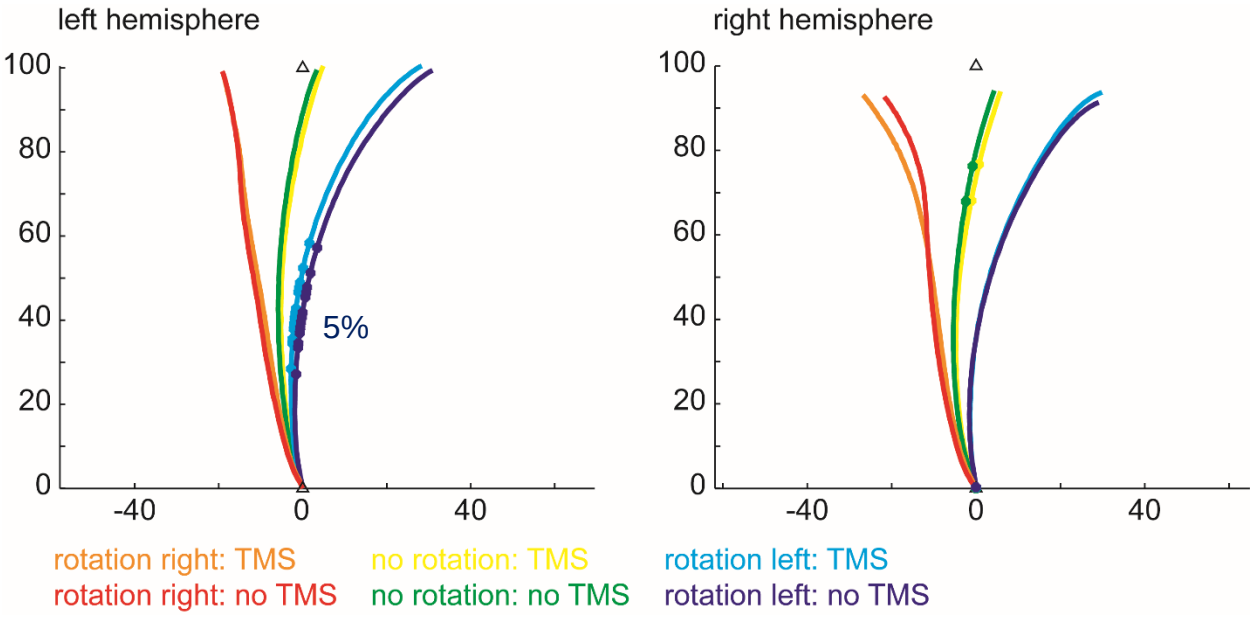

Figure S7 Average group trajectories for the TMS stimulation sites TPJ. Conventions analogue to Fig. S3. Note that the percentage indicates the proportion of **successive** significant tests.

S2.4 Main statistics without participating author

Comparison of the main TMS effects reported in 3.2 without the participating author.

	N = 10	***N = 9***
EndDevX over right IPS3 (rotation right)		
mean (SEM)	-23.2 (6.6) / -27.2 (6.4)	-22.0 (7.0) / -26.3 (7.3)
t-test	t_9 = 4.535; p = .001	t_8 = 4.564; p = .002
EndAng over right IPS3 (rotation right)		
mean (SEM)	-13.3 (3.1) / -16.2 (3.3)	-12.4 (3.3) / -15.6 (3.7)
t-test	t_9 = 3.741; p = .005	t_8 = 4.098; p = .003
EndDevX right IPS3 > all other sites	t_9 = 2.501; p = .017	t_8 = 2.368; p = .023

S2.5 Further exploratory analyses

In order to test whether the TMS effect we found might be mediated by differences in setup or motor behavior between subjects, we conducted some additional analyses on the condition with the robust TMS effect, the impairment of *EndDevX* during the rightward rotation when stimulating rIPS3. Specifically, we looked for a relationship between the visual angle of the target and the TMS effect on *EndDevX* but found no strong between-subject correlation (R^2 = 0.150; p = .269). The same negative result was obtained for the correlation between visual angle and effect on *EndVarX* (R^2 = 0.089; p = .403). Furthermore, neither the maximum reaching velocity (R^2 < 0.001; p = .955) nor total movement time (R^2 = 0.012; p = .764) revealed a relationship between the strength of the TMS effect and those kinematic measures.

Given that we do not find a relationship of these factors with the TMS effect in the condition with the strongest effect, it seems unlikely that any other site or dependent measure would be related with them.

S2.6 Detailed data and statistics

Mean summary statistics for the detailed conditions (mean (SEM)). Significant changes resulting from TMS stimulation are marked bold (uncorrected $\alpha = .05$) and red (Bonferroni corrected $\alpha = .005$).

		EndAng [°]	EndDevX	EndDevY	EndVarX	EndVarY	MT [ms]
left IPS1							
no rotation	TMS	4.5 (2.8)	7.9 (5.1)	105.9 (3.4)	11.3 (0.9)	9.6 (1.5)	985 (83)
	no TMS	5.4 (3.2)	9.3 (5.8)	101. (2.9)	12.1 (1.2)	8.7 (1.8)	975 (54)
	TMS effect	p = .404	p = .412	p = .054	p = .641	p = .326	p = .862
rotation left	TMS	17.5 (4.0)	31.7 (7.8)	97.3 (4.3)	20.8 (1.8)	15.8 (2.5)	1009 (44)
	no TMS	16.0 (4.9)	29.0 (9.2)	96.3 (3.7)	23.3 (3.6)	18.4 (4.0)	1038 (51)
	TMS effect	p = .396	p = .465	p = .660	p = .469	p = .615	p = .258
rotation right	TMS	-10.2 (5.4)	-20 (11.5)	10.9 (2.9)	20.8 (3.9)	14.4 (1.4)	1103 (60)
	no TMS	-10.1 (5.5)	-17.0 (10.1)	99.7 (4.4)	19.3 (5.3)	15.8 (2.2)	1109 (4)
	TMS effect	p = .930	p = .410	p = .323	p = .614	p = .323	p = .894
left IPS2							
no rotation	TMS	5.4 (2.4)	9.0 (4.0)	99.1 (3.6)	10.7 (2.3)	9.6 (2.1)	971 (54)
	no TMS	4.7 (2.5)	8.2 (4.4)	100.6 (3.8)	9.2 (1.1)	8.1 (0.7)	1025 (55)
	TMS effect	p = .229	p = .476	p = .360	p = .438	p = .362	p = .330
rotation left	TMS	16.9 (3.8)	30.4 (6.8)	97.5 (4.2)	20.4 (3.5)	14.6 (2.5)	1007 (33)
	no TMS	16.9 (3.5)	30.7 (6.8)	99.2 (4.6)	19.5 (3.5)	13.3 (2.0)	1022 (46)
	TMS effect	p = .981	p = .903	p = .330	p = .729	p = .434	p = .756
rotation right	TMS	-6.5 (4.9)	-11.7 (9.5)	103.7 (5.2)	18.6 (3.6)	18.6 (3.4)	1089 (59)
	no TMS	-7.4 (5.4)	-13.7 (11.3)	101.4 (5.3)	18.3 (3.5)	16.7 (1.8)	1086 (64)
	TMS effect	p = .424	p = .460	p = .240	p = .913	p = .401	p = .926
left IPS3							
no rotation	TMS	5.8 (2.9)	9.6 (4.8)	98.0 (4.1)	11.1 (1.5)	8.8 (0.8)	919 (48)
	no TMS	5.6 (3.0)	9.1 (5.1)	98.6 (3.7)	10.6 (1.4)	8.9 (1.3)	954 (56)
	TMS effect	p = .803	p = .736	p = .597	p = .729	p = .967	p = .286
rotation left	TMS	20.6 (4.1)	36.2 (7.1)	94.7 (4.6)	22.4 (2.0)	17.7 (2.5)	1001 (48)
	no TMS	19.0 (4.1)	32.6 (7.0)	94.4 (4.8)	21.3 (2.3)	15.3 (2.0)	1026 (49)
	TMS effect	p = .328	p = .240	p = .913	p = .451	p = .110	p = .577
rotation right	TMS	-9.6 (5.0)	-15.8 (8.7)	93.9 (4.4)	22.8 (4.8)	18.6 (5.1)	1004 (62)
	no TMS	-10.1 (5.3)	-19.6 (10.8)	98.9 (5.6)	19.4 (3.7)	17.2 (2.9)	1023 (53)
	TMS effect	p = .753	p = .343	p = .115	p = .219	p = .612	p = .676
left IPS4							
no rotation	TMS	3.9 (2.7)	6.6 (4.6)	99.7 (3.3)	10.5 (1.1)	10.2 (1.5)	931 (55)
	no TMS	2.2 (3.0)	3.4 (5.1)	99.3 (3.8)	12.3 (1.4)	12.0 (1.9)	930 (46)
	TMS effect	p = .087	p = .051	p = .735	**p = .030**	p = .105	p = .971
rotation left	TMS	14.0 (3.2)	24.8 (6.2)	98.1 (3.9)	22.5 (2.7)	16.8 (2.2)	953 (58)
	no TMS	14.8 (3.8)	26.8 (6.9)	98.0 (4.7)	16.3 (1.4)	15.5 (2.8)	962 (43)
	TMS effect	p = .546	p = .441	p = .971	**p = .011**	p = .518	p = .841
rotation right	TMS	-10.0 (4.7)	-18.0 (9.0)	102.4 (5.4)	18.6 (3.5)	22.1 (4.4)	1002 (38)
	no TMS	-9.9 (5.1)	-18.4 (10.2)	100.0 (5.3)	18.1 (3.3)	17.0 (3.3)	953 (66)
	TMS effect	p = .944	p = .617	p = .517	p = .617	**p = .034**	p = .249
left TPJ							
no rotation	TMS	3.1 (2.6)	5.2 (4.7)	101.2 (2.7)	11.8 (1.0)	8.3 (1.0)	938 (19)
	no TMS	2.2 (2.5)	3.7 (4.5)	100.3 (2.8)	11.1 (1.5)	8.8 (1.4)	937 (23)
	TMS effect	p = .224	p = .238	p = .127	p = .568	p = .598	p = .952
rotation left	TMS	15.6 (3.5)	29.9 (8.7)	100.8 (3.7)	17.5 (1.7)	13.7 (2.2)	974 (36)
	no TMS	17.4 (3.0)	26.9 (8.3)	99.6 (4.3)	18.0 (1.8)	13.0 (2.4)	1037 (51)
	TMS effect	p = .147	p = .243	p = .558	p = .810	p = .611	p = .070
rotation right	TMS	-11.2 (4.5)	-19.1 (8.6)	99.0 (4.6)	20.9 (5.0)	18.1 (5.1)	1072 (46)
	no TMS	-10.7 (3.9)	-19.4 (8.0)	99.8 (3.5)	21.3 (4.5)	15.1 (1.5)	1025 (39)
	TMS effect	p = .716	p = .884	p = .722	p = .891	p = .533	p = .204

		EndAng [°]	EndDevX	EndDevY	EndVarX	EndVarY	MT [ms]
right IPS1							
no rotation	TMS	2.8 (3.5)	4.2 (5.9)	97.1 (3.3)	9.2 (1.7)	7.9 (0.8)	978 (34)
	no TMS	3.1 (3.4)	4.8 (5.7)	96.8 (3.1)	8.4 (1.3)	12.0 (3.5)	965 (37)
	TMS effect	*p* = .773	*p* = .678	*p* = .848	*p* = .475	*p* = .236	*p* = .666
rotation left	TMS	16.5 (4.8)	29.9 (8.7)	96.6 (4.2)	17.9 (2.1)	13.4 (2.0)	1034 (38)
	no TMS	15.8 (4.9)	26.9 (8.3)	92.5 (3.9)	19.8 (3.3)	15.3 (2.5)	988 (36)
	TMS effect	*p* = .557	*p* = .370	***p* = .045**	*p* = .551	*p* = .222	*p* = .269
rotation right	TMS	-12.6 (2.9)	-21.8 (5.1)	100.0 (3.6)	18.1 (2.7)	18.1 (3.9)	1085 (53)
	no TMS	-11.9 (3.6)	-19.5 (5.9)	99.1 (7.3)	19.0 (2.6)	15.5 (2.1)	1078 (36)
	TMS effect	*p* = .741	*p* = .481	*p* = .627	*p* = .538	*p* = .456	*p* = .806
right IPS2							
no rotation	TMS	2.4 (3.5)	3.9 (6.0)	95.8 (3.0)	10.6 (1.2)	9.9 (2.5)	923 (72)
	no TMS	3.9 (3.9)	6.4 (6.6)	94.2 (2.5)	10.4 (1.0)	12.4 (2.6)	957 (43)
	TMS effect	***p* = .026**	***p* = .027**	*p* = .300	*p* = .833	*p* = .531	*p* = .494
rotation left	TMS	16.7 (5.7)	30.9 (10.4)	94.4 (3.4)	18.6 (3.0)	16.4 (3.1)	931 (96)
	no TMS	16.6 (5.2)	29.6 (9.0)	94.1 (3.8)	19.7 (3.3)	15.3 (2.1)	1002 (56)
	TMS effect	*p* = .942	*p* = .694	*p* = .883	*p* = .983	*p* = .458	*p* = .184
rotation right	TMS	-14.8 (3.3)	-25.9 (6.0)	97.5 (7.6)	18.3 (4.2)	14.3 (3.8)	1096 (62)
	no TMS	-15.0 (3.9)	-24.5 (6.4)	98.0 (8.2)	15.7 (1.9)	13.2 (1.8)	1101 (72)
	TMS effect	*p* = .889	*p* = .537	*p* = .779	*p* = .537	*p* = .731	*p* = .888
right IPS3							
no rotation	TMS	4.8 (3.8)	7.8 (6.3)	96.6 (3.6)	10.2 (1.7)	7.1 (1.1)	907 (89)
	no TMS	4.2 (3.6)	6.9 (6.0)	95.6 (2.8)	8.9 (1.4)	10.7 (2.4)	884 (89)
	TMS effect	*p* = .161	*p* = .258	*p* = .444	*p* = .280	*p* = .196	*p* = .365
rotation left	TMS	17.3 (5.6)	31.9 (9.6)	96.2 (6.0)	18.1 (2.5)	12.3 (2.5)	985 (86)
	no TMS	17.3 (5.3)	30.2 (8.9)	93.4 (4.5)	20.8 (5.1)	13.9 (2.5)	1007 (101)
	TMS effect	*p* = .990	*p* = .463	*p* = .263	*p* = .378	*p* = .401	*p* = .707
rotation right	TMS	-13.3 (3.1)	-23.2 (6.4)	99.9 (8.5)	17.3 (2.2)	16.3 (2.7)	1021 (104)
	no TMS	-16.2 (3.3)	-27.2 (6.6)	96.8 (8.4)	16.8 (3.4)	13.3 (1.8)	1031 (103)
	TMS effect	***p* = .005**	***p* = .001**	*p* = .216	*p* = .810	*p* = .312	*p* = .747
right IPS4							
no rotation	TMS	3.4 (3.1)	6.3 (5.7)	98.2 (3.2)	11.6 (1.8)	8.3 (1.0)	947 (69)
	no TMS	2.9 (3.3)	5.3 (5.7)	95.3 (3.0)	10.3 (1.4)	12.0 (3.4)	1010 (73)
	TMS effect	*p* = .488	*p* = .337	*p* = .100	*p* = .163	*p* = .327	*p* = .164
rotation left	TMS	15.6 (5.0)	28.2 (9.1)	93.3 (3.6)	20.0 (2.8)	13.7 (2.1)	1033 (51)
	no TMS	16.2 (5.0)	30.2 (9.5)	96.0 (4.3)	20.3 (3.3)	15.8 (2.1)	1033 (67)
	TMS effect	*p* = .532	*p* = .369	*p* = .222	*p* = .884	*p* = .326	*p* = .995
rotation right	TMS	-13.5 (3.0)	-23.0 (5.2)	101.5 (9.1)	21.7 (4.6)	17.1 (3.1)	1122 (95)
	no TMS	-16.2 (3.2)	-28.0 (6.2)	99.4 (9.5)	19.8 (4.3)	17.1 (2.7)	1112 (86)
	TMS effect	*p* = .175	*p* = .167	*p* = .359	*p* = .310	*p* = .996	*p* = .858
right TPJ							
no rotation	TMS	4.2 (3.3)	6.1 (5.1)	94.7 (4.1)	10.1 (1.1)	10.4 (2.3)	949 (46)
	no TMS	3.1 (3.2)	4.7 (5.0)	94.9 (3.8)	10.4 (2.0)	9.3 (2.0)	961 (49)
	TMS effect	*p* = .243	*p* = .190	*p* = .909	*p* = .817	*p* = .343	*p* = .654
rotation left	TMS	17.6 (5.2	30.5 (8.8)	93.9 (5.9)	16.8 (2.8)	17.2 (4.0)	1000 (35)
	no TMS	17.2 (5.4)	29.6 (9.0)	91.5 (4.8)	19.5 (3.5)	16.0 (2.4)	1015 (43)
	TMS effect	*p* = .790	*p* = .653	*p* = .211	*p* = .205	*p* = .647	*p* = .443
rotation right	TMS	-16.7 (3.8)	-27.3 (6.8)	93.5 (7.7)	21.4 (4.6)	18.3 (4.1)	1116 (61)
	no TMS	-13.4 (4.3)	-22.1 (7.4)	93.2 (6.8)	19.8 (2.3)	15.5 (2.1)	1130 (48)
	TMS effect	*p* = .123	*p* = .219	*p* = .814	*p* = .573	*p* = .297	*p* = .555

S2.7 Detailed analyses of across-trials variability

In order to test for TMS-induced increase in within-subject variability, we subjected the trajectory data to two additional analyses. First, we calculated the average correlation between the normalized x-positions for each subject and condition (see table below). This analysis did not reveal any TMS effects on the variability. Second, we calculated the within-subject SEM for each subject and condition and conducted an analysis analogue to the analysis of the mean trajectories (cf. S2.3). Figure 8 demonstrates that TMS only influenced the variability of rightward rotated trials when administered over the left TPJ. The effect however, a reduction in variability, is inconsistent with the hypothesis of a disruption of information processing by TMS.

Mean correlation coefficient for the detailed conditions (mean (SEM)). Significant changes resulting from TMS stimulation are marked bold (uncorrected $\alpha = .05$).

		left hemisphere			***right hemisphere***	
	TMS	no TMS	TMS effect (*p*)	TMS	no TMS	TMS effect (*p*)
IPS1						
no rotation	0.44 (0.07)	0.42 (0.07)	.680	0.54 (0.07)	0.55 (0.08)	.909
rotation left	0.44 (0.08)	0.42 (0.09)	.584	0.43 (0.11)	0.36 (0.10)	.266
rotation right	0.49 (0.10)	0.49 (0.11)	.941	0.41 (0.10)	0.39 (0.10)	.831
IPS2						
no rotation	0.36 (0.08)	0.41 (0.09)	.482	0.41 (0.08)	0.42 (0.10)	.686
rotation left	0.50 (0.08)	0.51 (0.12)	.906	0.45 (0.10)	0.48 (0.10)	.594
rotation right	0.50 (0.11)	0.52 (0.12)	.585	0.42 (0.10)	0.48 (0.08)	.118
IPS3						
no rotation	0.44 (0.04)	0.47 (0.05)	.642	0.50 (0.10)	0.48 (0.10)	.558
rotation left	0.52 (0.07)	0.43 (0.10)	.252	0.56 (0.10)	0.44 (0.09)	.269
rotation right	0.45 (0.08)	0.51 (0.10)	.554	0.50 (0.11)	0.51 (0.10)	.480
IPS4						
no rotation	0.39 (0.09)	0.39 (0.09)	.891	0.43 (0.08)	0.45 (0.09)	.738
rotation left	0.31 (0.09)	0.43 (0.09)	**.028**	0.41 (0.10)	0.40 (0.11)	.647
rotation right	0.46 (0.10)	0.52 (0.12)	.485	0.44 (0.12)	0.54 (0.10)	.074
TPJ						
no rotation	0.33 (0.08)	0.30 (0.08)	.550	0.40 (0.11)	0.36 (0.10)	.271
rotation left	0.48 (0.08)	0.50 (0.08)	.615	0.42 (0.09)	0.35 (0.10)	.190
rotation right	0.44 (0.09)	0.43 (0.09)	.887	0.44 (0.09)	0.31 (0.12)	.154

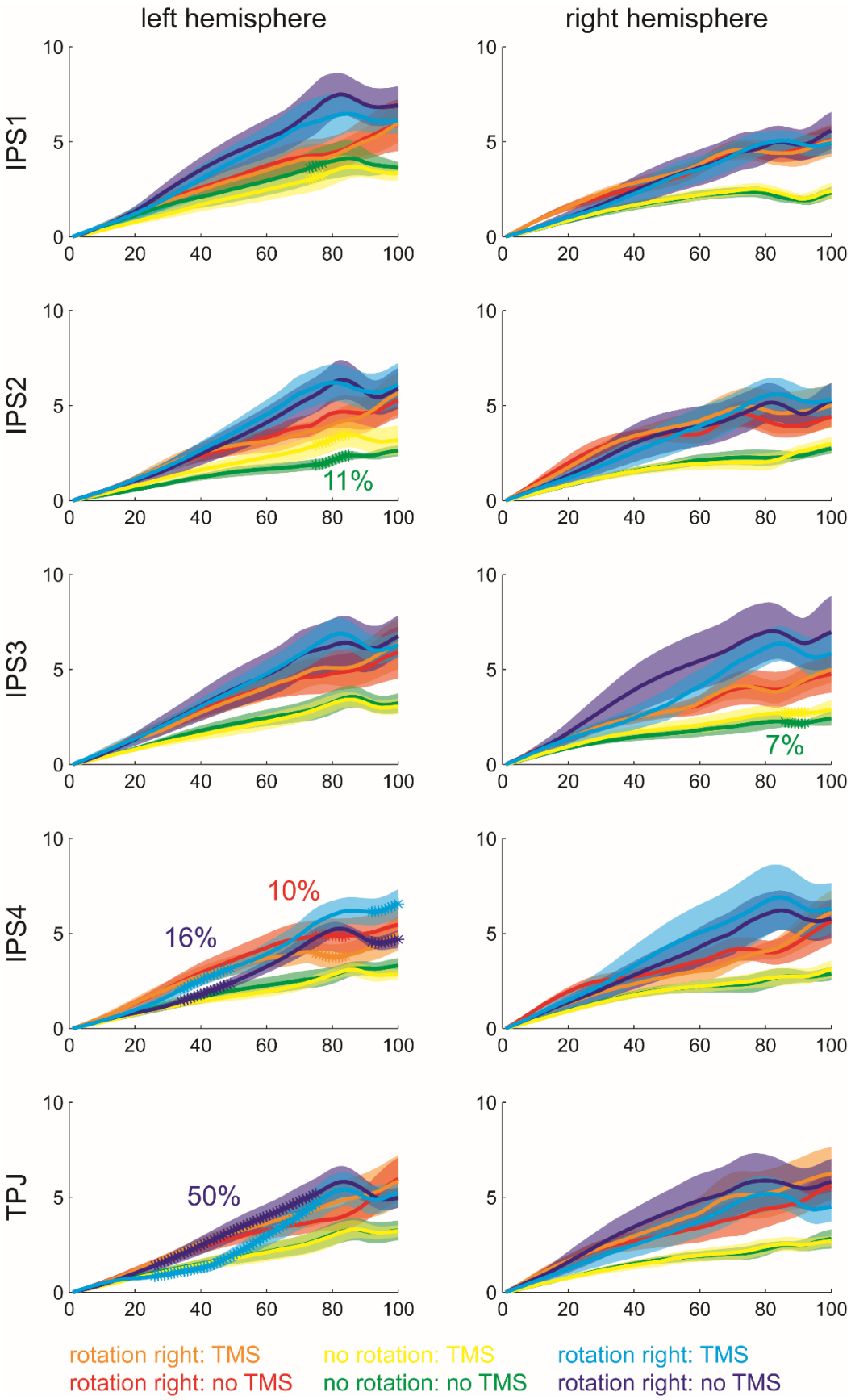
left hemisphere
right hemisphere
IPS1
IPS2
IPS3
IPS4
TPJ
11%
7%
10%
16%
50%
rotation right: TMS
rotation right: no TMS
no rotation: TMS
no rotation: no TMS
rotation right: TMS
rotation right: no TMS

Figure S8 Average within-subject SEM in x direction along the trajectories. The x-axes denotes the 100 segments to which the data is normalized, and the y-axis the SEM in spatially normalized arbitrary units The stars / bold parts indicate the positions where the SEM differed significantly between TMS and no TMS trials across participants ($p < .05$, uncorrected). Note that the percentages indicate the proportion of **successive** significant tests.

S3. Supplementary References

Chib, V.S., Krutky, M.A., Lynch, K.M., Mussa-Ivaldi, F.A., 2009. The separate neural control of hand movements and contact forces. J Neurosci 29, 3939-3947.

Della-Maggiore, V., Malfait, N., Ostry, D.J., Paus, T., 2004. Stimulation of the posterior parietal cortex interferes with arm trajectory adjustments during the learning of new dynamics. J Neurosci 24, 9971-9976.

Dieterich, M., Bense, S., Lutz, S., Drzezga, A., Stephan, T., Bartenstein, P., Brandt, T., 2003. Dominance for vestibular cortical function in the non-dominant hemisphere. Cereb Cortex 13, 994-1007.

Grefkes, C., Fink, G.R., 2005. The functional organization of the intraparietal sulcus in humans and monkeys. J Anat 207, 3-17.

Mazziotta, J., Toga, A., Evans, A., Fox, P., Lancaster, J., Zilles, K., Woods, R., Paus, T., Simpson, G., Pike, B., Holmes, C., Collins, L., Thompson, P., MacDonald, D., Iacoboni, M., Schormann, T., Amunts, K., Palomero-Gallagher, N., Geyer, S., Parsons, L., Narr, K., Kabani, N., Le Goualher, G., Boomsma, D., Cannon, T., Kawashima, R., Mazoyer, B., 2001. A probabilistic atlas and reference system for the human brain: International Consortium for Brain Mapping (ICBM). Philos Trans R Soc Lond B Biol Sci 356, 1293-1322.

Okamoto, M., Dan, H., Sakamoto, K., Takeo, K., Shimizu, K., Kohno, S., Oda, I., Isobe, S., Suzuki, T., Kohyama, K., Dan, I., 2004. Three-dimensional probabilistic anatomical cranio-cerebral correlation via the international 10-20 system oriented for transcranial functional brain mapping. Neuroimage 21, 99-111.

Reichenbach, A., Bresciani, J.P., Peer, A., Bülthoff, H.H., Thielscher, A., 2011. Contributions of the PPC to online control of visually guided reaching movements assessed with fMRI-guided TMS. Cereb Cortex 21, 1602-1612.

Reichenbach, A., Thielscher, A., Peer, A., Bülthoff, H.H., Bresciani, J.P., 2014. A key region in the human parietal cortex for processing proprioceptive hand feedback during reaching movements. Neuroimage 84, 615-625.

Schomaker, J., Tesch, J., Bulthoff, H.H., Bresciani, J.P., 2011. It is all me: the effect of viewpoint on visual-vestibular recalibration. Exp Brain Res 213, 245-256.

Seemungal, B.M., Rizzo, V., Gresty, M.A., Rothwell, J.C., Bronstein, A.M., 2008. Posterior parietal rTMS disrupts human Path Integration during a vestibular navigation task. Neurosci Lett 437, 88-92.

Smith, S.M., Beckmann, C.F., Ramnani, N., Woolrich, M.W., Bannister, P.R., Jenkinson, M., Matthews, P.M., McGonigle, D.J., 2005. Variability in fMRI: a re-examination of inter-session differences. Hum Brain Mapp 24, 248-257.

Smith, S.M., Jenkinson, M., Woolrich, M.W., Beckmann, C.F., Behrens, T.E., Johansen-Berg, H., Bannister, P.R., De Luca, M., Drobnjak, I., Flitney, D.E., Niazy, R.K., Saunders, J., Vickers, J., Zhang, Y., De Stefano, N., Brady, J.M., Matthews, P.M., 2004. Advances in functional and structural MR image analysis and implementation as FSL. Neuroimage 23 Suppl 1, S208-219.

Stephan, T., Deutschlander, A., Nolte, A., Schneider, E., Wiesmann, M., Brandt, T., Dieterich, M., 2005. Functional MRI of galvanic vestibular stimulation with alternating currents at different frequencies. Neuroimage 26, 721-732.

Suzuki, M., Kitano, H., Ito, R., Kitanishi, T., Yazawa, Y., Ogawa, T., Shiino, A., Kitajima, K., 2001. Cortical and subcortical vestibular response to caloric stimulation detected by functional magnetic resonance imaging. Brain Res Cogn Brain Res 12, 441-449.